Journal of Computational Applied Mechanics 2026, 57(2): 348-361

DOI: 10.22059/jcamech.2026.410501.1775

RESEARCH PAPER

Dynamic response of porosity-dependent FG nanoplate based on nonlocal strain-stress gradient theory

Hela D. El-Shahrany [a], Ashraf M. Zenkour [b,c,*]

[a] Department of Mathematics, Faculty of Science, University of Bisha, P.O. Box 344, Bisha 61922, Saudi Arabia
[b] Department of Mathematics, Faculty of Science, King Abdulaziz University, P.O. Box 80203, Jeddah 21589, Saudi Arabia
[c] Department of Mathematics, Faculty of Science, Kafrelsheikh University, Kafrelsheikh 33516, Egypt

Abstract

This study investigates the free vibration behavior of porous functionally graded plates (PFGPs) within the context of nonlocal strain–gradient elasticity theory. Two different porosity distribution types are examined, and the thickness-wise variation of material properties is modeled by means of an enhanced power-law scheme. The kinematic description is formulated based on a refined higher-order shear deformation plate theory that inherently enforces zero transverse shear stresses at the plate surfaces, thus evading the usage of shear correction factors. The governing equations of motion for the nonlocal model are derived via Hamilton's principle and explained analytically to get the natural frequencies of the PFGPs. A detailed parametric analysis is performed to assess the effects of the nonlocal parameter, internal material length scale, power-law exponent, wave number, and porosity parameters on the vibrational characteristics. The validity and effectiveness of the current preparation are confirmed through comparisons with existing results obtainable in the literature.

Keywords: Functionally graded plate; porosity; nonlocal strain-stress gradient theory (NSGT); higher-order normal and shear deformations theory

1. Introduction

Functionally graded materials (FGMs) have been developed to meet the growing demands of advanced engineering applications due to their superior mechanical and thermal characteristics, such as enhanced resistance to oxidation, corrosion, and high-temperature environments. These materials belong to a class of composite structures in which material constituents vary continuously through the thickness, resulting in a smooth transition of properties and reduced stress concentrations compared with conventional layered composites.

Extensive research has been dedicated to the mechanical actions of FGM-based structures using high-order shear deformation theories, including bending, buckling, and vibration. Early contributions by Reddy and co-workers [1-3] employed third-order shear deformation theory to investigate the responses of isotropic and FG beams and plates. Subsequently, numerous refined shear deformation models were proposed to achieve more accurate representations of transverse shear effects through various shape functions, such as trigonometric, hyperbolic, exponential,

* Corresponding author.E-mail address: zenkour@kau.edu.sa

exponential–logarithmic, trigonometric–exponential, and polynomial forms [4-27].

During the fabrication of FGMs, imperfections such as porosity may arise, significantly influencing stiffness and overall mechanical performance and increasing susceptibility to damage. Consequently, incorporating porosity effects into structural modelling has become essential. Several studies have addressed this issue by examining the mechanical responses of porous FGM structures. El-shahrany [27] analyzed the normal and shear deformations of unidirectional and bi-directional porous FGM nano plate with three constituents, employing hyperbolic shear/normal deformations theory and Eringen's nonlocal elasticity theory. Cuong-Le et al. [28] examined buckling and free vibration of porous FG annular plate and shell structures with graded porosity distributions. Slimane et al. [29] and Kenanda et al. [30] explored the impact of the porosity distributions and thickness stretching on the vibration behaviour of smart FG-based plates. Additional works have employed high-order and quasi-3D theories to capture the coupled impacts of shear deformations, thickness stretching, and porosity on dynamic responses [31-33]. Moreover, Pham et al. [34] used the Rayleigh–Ritz method and Chebyshev polynomials to discuss the hygro-thermo-mechanical loading effect on behaviour of the porous functionally graded curved nano beam rested on an elastic foundation.

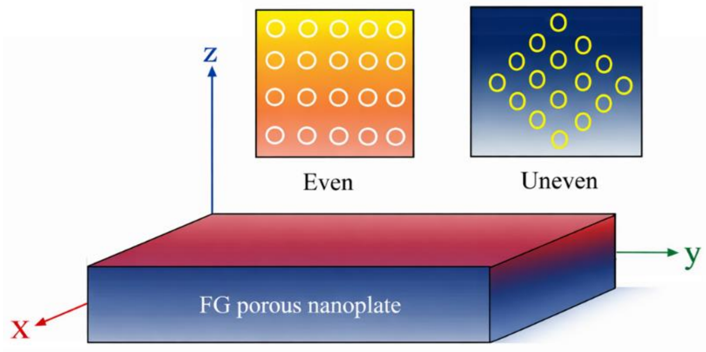

Fig 1: A dimensional configuration of the proposed porous FG plate

2. Theoretical nonlocal strain-stress gradient theory

The stresses take into account the influences of nonlocal-elastic stresses besides strain gradient stresses according to the NSGT. Then, the stress field can be expressed as [33]

$$\sigma_{ij} = \sigma_{ij}^{(0)} - \nabla\sigma_{ij}^{(1)}, \tag{1}$$

in which the classical stresses $\sigma_{ij}^{(0)}$ can be displayed as

$$\sigma_{ij}^{(0)} = \int_0^L \tilde{c}_{ijkl}\alpha_0(\boldsymbol{x}, \boldsymbol{x}', e_0 a)\varepsilon'_{kl}(\boldsymbol{x}')\mathrm{d}\boldsymbol{x}', \tag{2}$$

and the high-order nonlocal stresses $\sigma_{ij}^{(1)}$ can be expressed as

$$\sigma_{ij}^{(1)} = l^2 \int_0^L \tilde{c}_{ijkl}\alpha_1(\boldsymbol{x}, \boldsymbol{x}', e_1 a)\varepsilon'_{kl,1}(\boldsymbol{x}')\mathrm{d}\boldsymbol{x}', \tag{3}$$

where $\tilde{c}_{ijkl}$ represents the elastic coefficient and $e_i a$, $i = 0,1$ are the nonlocality parameters. The parameter l accounts for the strain gradient impacts. The following equation describes the constitutive relation of NSGT [32]:

$$[1-(e_0 a)^2\nabla^2][1-(e_1 a)^2\nabla^2]\sigma_{ij} = \tilde{c}_{ijkl}\{[1-(e_1 a)^2\nabla^2]\varepsilon_{kl} - l^2[1-(e_0 a)^2\nabla^2]\nabla^2\varepsilon_{kl}\}, \tag{4}$$

where $\nabla^2 = \partial_x^2 + \partial_y^2$. Consider $e_0 = e_1 = e$ and $\mu = ea$, hence

$$(1-\mu^2\nabla^2)\sigma_{ij} = \tilde{c}_{ijkl}(1-l^2\nabla^2)\varepsilon_{kl}. \tag{5}$$

Furthermore, the constitutive relations in Eq. (5) can be simplified to the following cases:

- By putting $l = 0$ in Eq. (5), the constitutive model of the non-local elasticity theory [35] can be given as

$$(1-\mu^2\nabla^2)\sigma_{ij} = \tilde{c}_{ijkl}\varepsilon_{kl}. \tag{6}$$

- By putting $\mu = 0$ in Eq. (5), the constitutive model of the strain gradient theory can be obtained as

$$\sigma_{ij} = \tilde{c}_{ijkl}(1 - l^2\nabla^2)\varepsilon_{kl}. \tag{7}$$

3. PFG-based material properties

A porous rectangular plate of FG material with a thickness h, a length a, and a width b containing the top ceramic surface and the bottom metal surface, as seen in Fig. 1. A following power-law function is employed to describe the porous FG plate properties, including mass density ρ, the elastic modulus E as

$$\eta(x_3) = \eta_m + (\eta_c - \eta_m)\left(\frac{z}{h} + \frac{1}{2}\right)^p + \chi, \tag{8}$$

where p is the power law, respectively. Moreover, the term χ can be determined for a perfect FGM as $\chi = 0$, for even distribution of porosity as $\chi = -\frac{\beta}{2}(\eta_c + \eta_m)$, $0 \leq \beta \leq 1$, and for uneven distribution of porosity as $\chi = -\frac{\beta}{2}(\eta_c + \eta_m)\left(1 - \frac{2|z|}{h}\right)$, where β is the porosity constant.

3.1. Problem formulation

By considering the effect of the thickness extension, the displacements can be represented as

$$\begin{gathered} U_1(x,y,z,t) = u_1(x,y,t) - z\frac{\partial u_3}{\partial x} + F(z)\phi_1(x,y,t), \\ U_2(x,y,z,t) = u_2(x,y,t) - z\frac{\partial u_3}{\partial y} + F(z)\phi_2(x,y,t), \\ U_3(x,y,z,t) = u_3(x,y,t) + F'(z)\phi_3(x,y,t), \\ F(z) = h\sinh(z/h) - (4z^3/3h^2)\cosh(1/2), \end{gathered} \tag{9}$$

where u_1, u_2, and u_3 are the mid-plane displacement components and ϕ_i, i =1, 2, and 3 are the rotation components along the x, y, and z directions.

The linear strains of a porous system are defined as

$$\begin{gathered} \varepsilon_x = \frac{\partial u_1}{\partial x} - z\frac{\partial^2 u_3}{\partial x^2} + F(z)\frac{\partial \phi_1}{\partial x}, \quad \varepsilon_y = \frac{\partial u_2}{\partial y} - z\frac{\partial^2 u_3}{\partial y^2} + F(z)\frac{\partial \phi_2}{\partial y}, \quad \varepsilon_z = F''(z)\phi_3, \\ \gamma_{yz} = F'(z)\left(\phi_2 + \frac{\partial \phi_3}{\partial y}\right), \quad \gamma_{xz} = F'(z)\left(\phi_1 + \frac{\partial \phi_3}{\partial x}\right), \quad \gamma_{xy} = \frac{\partial u_1}{\partial y} + \frac{\partial u_2}{\partial x} - 2z\frac{\partial^2 u_3}{\partial x \partial y} + F(z)\left(\frac{\partial \phi_1}{\partial y} + \frac{\partial \phi_2}{\partial x}\right). \end{gathered} \tag{10}$$

Hooke's law describes the relationship between the stresses and the strains as

$$(1 - \mu^2\nabla^2)\bar{\sigma} = \tilde{c}_{ij}(1 - l^2\nabla^2)\bar{\varepsilon}, \tag{11}$$

in which

$$\bar{\sigma} = \{\sigma_x, \sigma_y, \sigma_z, \tau_{yz}, \tau_{xz}, \tau_{xy}\}^T, \quad \bar{\varepsilon} = \{\varepsilon_x, \varepsilon_y, \varepsilon_z, \gamma_{yz}, \gamma_{xz}, \gamma_{xy}\}^T, \quad \tilde{c}_{ij} = \begin{bmatrix} \tilde{c}_{11} & \tilde{c}_{12} & \tilde{c}_{13} & 0 & 0 & 0 \\ \tilde{c}_{21} & \tilde{c}_{22} & \tilde{c}_{23} & 0 & 0 & 0 \\ \tilde{c}_{31} & \tilde{c}_{32} & \tilde{c}_{33} & 0 & 0 & 0 \\ 0 & 0 & 0 & \tilde{c}_{44} & 0 & 0 \\ 0 & 0 & 0 & 0 & \tilde{c}_{55} & 0 \\ 0 & 0 & 0 & 0 & 0 & \tilde{c}_{66} \end{bmatrix}. \tag{12}$$

The stiffness coefficients $\tilde{c}_{ij}$ are given by:

$$\tilde{c}_{11} = \tilde{c}_{22} = \tilde{c}_{33} = \frac{E(z)(1-\nu)}{(1-2\nu)(1+\nu)}, \quad \tilde{c}_{12} = \tilde{c}_{13} = \tilde{c}_{23} = \frac{\nu E(z)}{(1-2\nu)(1+\nu)}, \quad \tilde{c}_{44} = \tilde{c}_{55} = \tilde{c}_{66} = G(z) = \frac{E(z)}{2(1+\nu)}, \tag{13}$$

where $E(z)$, ν, and $G(z)$ are Young's modulus, Poisson's ratio, and shear modulus of the porous system, respectively.

3.2. Motion system

Based on Hamilton's principle, the motion system can be given by the next variation form:

$$\int_0^t (\delta E_s + \delta E_p - \delta E_k)\, \mathrm{d}t = 0, \tag{14}$$

$$\delta E_s = \int_V \left(\sigma_x \delta\varepsilon_x + \sigma_y \delta\varepsilon_y + \sigma_z \delta\varepsilon_z + \tau_{yz}\delta\gamma_{yz} + \tau_{xz}\delta\gamma_{xz} + \tau_{xy}\delta\gamma_{xy}\right) \mathrm{d}V, \tag{15}$$

$$\delta E_p = -\int_A q\delta w \, \mathrm{d}A, \tag{16}$$

$$\delta E_k = \int_V \left(\dot{U}_1\delta\dot{U}_1 + \dot{U}_2\delta\dot{U}_2 + \dot{U}_3\delta\dot{U}_3\right)\rho(z)\, \mathrm{d}V, \tag{17}$$

in which δE_p, δE_s and δE_k calculate variations of the three energies: the potential energy of the applied loads, the strain energy, and the kinetic energy, respectively.

By using Eqs. (15)-(17) into Eq. (14) and substituting Eqs. (11)-(13) in (14). The motion system is obtained as:

$$\begin{aligned}
&\delta u_1: (1-l^2\nabla^2)\left(\frac{\partial N_x}{\partial x} + \frac{\partial N_{xy}}{\partial y}\right) = (1-\mu^2\nabla^2)\left(T_1\ddot{u}_1 - T_2\frac{\partial \ddot{u}_3}{\partial x} + T_4\ddot{\phi}_1\right),\\
&\delta u_2: (1-l^2\nabla^2)\left(\frac{\partial N_{xy}}{\partial x} + \frac{\partial N_y}{\partial y}\right) = (1-\mu^2\nabla^2)\left(T_1\ddot{u}_2 - T_2\frac{\partial \ddot{u}_3}{\partial y} + T_4\ddot{\phi}_2\right),\\
&\delta u_3: (1-l^2\nabla^2)\left(\frac{\partial^2 M_x}{\partial x^2} + 2\frac{\partial^2 M_{xy}}{\partial x\partial y} + \frac{\partial^2 M_y}{\partial y^2}\right) = (1-\mu^2\nabla^2)\Big[T_1\ddot{u}_3 + T_2\left(\frac{\partial \ddot{u}_1}{\partial x} + \frac{\partial \ddot{u}_2}{\partial y}\right) - T_3\left(\frac{\partial^2 \ddot{u}_3}{\partial x^2} + \frac{\partial^2 \ddot{u}_3}{\partial y^2}\right) +\\
&\qquad T_5\left(\frac{\partial \ddot{\phi}_1}{\partial x} + \frac{\partial \ddot{\phi}_2}{\partial y}\right) + T_7\ddot{\phi}_3\Big],\\
&\delta \phi_1: (1-l^2\nabla^2)\left(\frac{\partial S_x}{\partial x} + \frac{\partial S_{xy}}{\partial y} - Q_{x_{13}}\right) = (1-\mu^2\nabla^2)\left(T_4\ddot{u}_1 - T_5\frac{\partial \ddot{u}_3}{\partial x} + T_6\ddot{\phi}_1\right),\\
&\delta \phi_2: (1-l^2\nabla^2)\left(\frac{\partial S_{xy}}{\partial x} + \frac{\partial S_y}{\partial y} - Q_{yz}\right) = (1-\mu^2\nabla^2)\left(T_4\ddot{u}_2 - T_5\frac{\partial \ddot{u}_3}{\partial y} + T_6\ddot{\phi}_2\right),\\
&\delta \phi_3: (1-l^2\nabla^2)\left(\frac{\partial Q_{xz}}{\partial x} + \frac{\partial Q_{yz}}{\partial y} - N_z\right) = (1-\mu^2\nabla^2)\left(T_7\ddot{u}_3 + T_8\ddot{\phi}_3\right),
\end{aligned} \tag{18}$$

where N, M, S, and Q are the moment and the stress resultants, while T_i, $i = 1, \ldots, 8$ represent the moments of inertia, which are mentioned in Appendix A. The system (18) can be rewritten as:

$$\begin{aligned}
&\delta u_1: (1-l^2\nabla^2)\Big\{A_{11}\frac{\partial^2 u_1}{\partial x^2} - B_{11}\frac{\partial^3 u_3}{\partial x^3} + V_{11}\frac{\partial^2 \phi_1}{\partial x^2} + A_{12}\frac{\partial^2 u_2}{\partial x\partial y} - B_{12}\frac{\partial^3 u_3}{\partial x\partial y^2} + V_{12}\frac{\partial^2 \phi_2}{\partial x\partial y} +\\
&\qquad D_{13}\frac{\partial \phi_3}{\partial x} + A_{66}\frac{\partial^2 u_1}{\partial y^2} + A_{66}\frac{\partial^2 u_2}{\partial x\partial y} - 2B_{66}\frac{\partial^3 u_3}{\partial x\partial y^2} + V_{66}\left(\frac{\partial^2 \phi_1}{\partial y^2} + \frac{\partial^2 \phi_2}{\partial x\partial y}\right)\Big\}\\
&\qquad = (1-\mu^2\nabla^2)\left(T_1\ddot{u}_1 - T_2\frac{\partial \ddot{u}_3}{\partial x} + T_4\ddot{\phi}_1\right),
\end{aligned} \tag{19}$$

$$\begin{aligned}
&\delta u_2: (1-l^2\nabla^2)\Big\{A_{66}\frac{\partial^2 u_1}{\partial x\partial y} + A_{66}\frac{\partial^2 u_2}{\partial x^2} - 2B_{66}\frac{\partial^3 u_3}{\partial x^2\partial y} + V_{66}\left(\frac{\partial^2 \phi_1}{\partial x\partial y} + \frac{\partial^2 \phi_2}{\partial x^2}\right) + A_{21}\frac{\partial^2 u_1}{\partial x\partial y} - B_{21}\frac{\partial^3 u_3}{\partial x^2\partial x_2}\\
&+V_{21}\frac{\partial^2 \phi_1}{\partial x\partial y} + A_{22}\frac{\partial^2 u_2}{\partial y^2} - B_{22}\frac{\partial^3 u_3}{\partial y^3} + V_{22}\frac{\partial^2 \phi_2}{\partial y^2} + D_{23}\frac{\partial \phi_3}{\partial y}\Big\} = (1-\mu^2\nabla^2)\left(T_1\ddot{u}_2 - T_2\frac{\partial \ddot{u}_3}{\partial y} + T_4\ddot{\phi}_2\right),
\end{aligned} \tag{20}$$

$$\begin{aligned}
&\delta u_3: (1-l^2\nabla^2)\Big\{B_{11}\frac{\partial^3 u_1}{\partial x^3} - E_{11}\frac{\partial^4 u_3}{\partial x^4} + F_{11}\frac{\partial^3 \phi_1}{\partial x^3} + B_{12}\frac{\partial^3 u_2}{\partial x^2\partial y} - E_{12}\frac{\partial^4 u_3}{\partial x^2\partial y^2} + F_{12}\frac{\partial^3 \phi_2}{\partial x^2\partial y} +\\
&\quad G_{13}\frac{\partial^2 \phi_3}{\partial x^2} + 2B_{66}\frac{\partial^3 u_1}{\partial x\partial y^2} + 2B_{66}\frac{\partial^3 u_2}{\partial x^2\partial y} - 4E_{66}\frac{\partial^4 u_3}{\partial x^2\partial y^2} + 2F_{66}\left(\frac{\partial^3 \phi_1}{\partial x\partial y^2} + \frac{\partial^3 \phi_2}{\partial x^2\partial y}\right) + B_{21}\frac{\partial^3 u_1}{\partial x\partial y^2}\\
&\quad -E_{21}\frac{\partial^4 u_3}{\partial x^2\partial y^2} + F_{21}\frac{\partial^3 \phi_1}{\partial x\partial y^2} + B_{22}\frac{\partial^3 u_2}{\partial y^3} - E_{22}\frac{\partial^4 u_3}{\partial y^4} + F_{22}\frac{\partial^3 \phi_2}{\partial y^3} + G_{23}\frac{\partial^2 \phi_3}{\partial y^2}\Big\}\\
&= (1-\mu^2\nabla^2)\left[T_1\ddot{u}_3 + T_2\left(\frac{\partial \ddot{u}_1}{\partial x} + \frac{\partial \ddot{u}_2}{\partial y}\right) - T_3\left(\frac{\partial^2 \ddot{u}_3}{\partial x^2} + \frac{\partial^2 \ddot{u}_3}{\partial y^2}\right) + T_5\left(\frac{\partial \ddot{\phi}_1}{\partial x} + \frac{\partial \ddot{\phi}_2}{\partial y}\right) + T_7\ddot{\phi}_3\right],
\end{aligned} \tag{21}$$

$$\begin{aligned}
&\delta \phi_1: (1-l^2\nabla^2)\Big\{V_{11}\frac{\partial^2 u_1}{\partial x^2} - F_{11}\frac{\partial^3 u_3}{\partial x^3} + H_{11}\frac{\partial^2 \phi_1}{\partial x^2} + V_{12}\frac{\partial^2 u_2}{\partial x\partial y} - F_{12}\frac{\partial^3 u_3}{\partial x\partial y^2} + H_{12}\frac{\partial^2 \phi_2}{\partial x\partial y} +\\
&+K_{13}\frac{\partial \phi_3}{\partial x} + V_{66}\left(\frac{\partial^2 u_1}{\partial y^2} + \frac{\partial^2 u_2}{\partial x\partial y}\right) - 2F_{66}\frac{\partial^3 u_3}{\partial x\partial y^2} + H_{66}\left(\frac{\partial^2 \phi_1}{\partial y^2} + \frac{\partial^2 \phi_2}{\partial x\partial y}\right) - M_{55}\left(\phi_1 + \frac{\partial \phi_3}{\partial x}\right)\Big\}\\
&\qquad = (1-\mu^2\nabla^2)\left(T_4\ddot{u}_1 - T_5\frac{\partial \ddot{u}_3}{\partial x} + T_6\ddot{\phi}_1\right),
\end{aligned} \tag{22}$$

$$\begin{aligned}
&\delta \phi_2: (1-l^2\nabla^2)\Big\{V_{66}\left(\frac{\partial^2 u_1}{\partial x\partial y} + \frac{\partial^2 u_2}{\partial x^2}\right) - 2F_{66}\frac{\partial^3 u_3}{\partial x^2\partial y} + H_{66}\left(\frac{\partial^2 \phi_1}{\partial x\partial y} + \frac{\partial^2 \phi_2}{\partial y^2}\right) + V_{21}\frac{\partial^2 u_1}{\partial x\partial y} - F_{21}\frac{\partial^3 u_3}{\partial x^2\partial y} +\\
&\qquad H_{21}\frac{\partial^2 \phi_1}{\partial x\partial y} + V_{22}\frac{\partial^2 u_2}{\partial y^2} - F_{22}\frac{\partial^3 u_3}{\partial y^3} + H_{22}\frac{\partial^2 \phi_2}{\partial y^2} + K_{23}\frac{\partial \phi_3}{\partial y} - M_{44}\left(\phi_2 + \frac{\partial \phi_3}{\partial y}\right)\Big\}\\
&\qquad = (1-\mu^2\nabla^2)\left(T_4\ddot{u}_2 - T_5\frac{\partial \ddot{u}_3}{\partial y} + T_6\ddot{\phi}_2\right),
\end{aligned} \tag{23}$$

$$\delta\phi_3:(1-l^2\nabla^2)\Big\{M_{55}\Big(\frac{\partial\phi_1}{\partial x}+\frac{\partial^2\phi_3}{\partial x^2}\Big)+M_{44}\Big(\frac{\partial\phi_2}{\partial y}+\frac{\partial^2\phi_3}{\partial y^2}\Big)-D_{31}\frac{\partial u_1}{\partial x}+G_{31}\frac{\partial^2 u_3}{\partial x^2}-K_{31}\frac{\partial\phi_1}{\partial x}$$
$$-D_{32}\frac{\partial u_2}{\partial y}+G_{32}\frac{\partial^2 u_3}{\partial y^2}-K_{32}\frac{\partial\phi_2}{\partial y}-L_{33}\phi_3\Big\}=(1-\mu^2\nabla^2)\big(T_7\ddot{u}_3+T_8\ddot{\phi}_3\big). \tag{24}$$

3.3. Analytical solution

By employing the double Fourier series and Navier's approach, solutions of the equations system that describe the simply-supported PFG plate are expanded

$$\begin{Bmatrix}u_1\\u_2\\u_3\\\phi_1\\\phi_2\\\phi_3\end{Bmatrix}=\sum_{m=1}^{\infty}\sum_{n=1}^{\infty}\begin{Bmatrix}U_{1mn}\cos(\lambda_1x)\sin(\lambda_2y)\\U_{2mn}\sin(\lambda_1x)\cos(\lambda_2y)\\U_{3mn}\sin(\lambda_1x)\sin(\lambda_2y)\\\Phi_{1mn}\cos(\lambda_1x)\sin(\lambda_2y)\\\Phi_{2mn}\sin(\lambda_1x)\cos(\lambda_2y)\\\Phi_{3mn}\sin(\lambda_1x)\sin(\lambda_2y)\end{Bmatrix}\mathrm{e}^{i\omega_{mn}t},\quad \lambda_1=m\pi/a,\quad \lambda_2=n\pi/b. \tag{25}$$

The coefficients U_{1mn}, U_{2mn}, U_{3mn}, Φ_{1mn}, Φ_{2mn}, and Φ_{3mn} must be determined. The coefficient ω_{mn} represents the frequency of (m,n) wavenumbers. Using Fourier's forms in Eq. (24) in Eqs. (19)-(23) to obtain

$$\begin{gathered}
\big([S_{ij}]-\omega^2[P_{ij}]\big)\{\Delta\}=0,\quad i=1,\dots,6,\quad \{\Delta\}=\{U_{1mn},U_{2mn},U_{3mn},\Phi_{1mn},\Phi_{2mn},\Phi_{3mn}\}^T,\\
S_{11}=-[1+l^2(\lambda_1^2+\lambda_2^2)](A_{11}\lambda_1^2+A_{66}\lambda_2^2),\quad S_{22}=-[1+l^2(\lambda_1^2+\lambda_2^2)](A_{66}\lambda_1^2+A_{22}\lambda_2^2),\\
S_{33}=-[1+l^2(\lambda_1^2+\lambda_2^2)][E_{11}\lambda_1^4+\lambda_1^2\lambda_2^2(2E_{12}+4E_{66})+E_{22}\lambda_2^4],\\
S_{44}=-[1+l^2(\lambda_1^2+\lambda_2^2)](M_{55}+H_{11}\lambda_1^2+H_{66}\lambda_2^2),\quad S_{55}=-[1+l^2(\lambda_1^2+\lambda_2^2)](M_{44}+H_{22}\lambda_2^2+H_{66}\lambda_1^2),\\
S_{66}=[1+l^2(\lambda_1^2+\lambda_2^2)](L_{33}-M_{55}\lambda_1^2-M_{44}\lambda_2^2),\quad S_{12}=-\lambda_1\lambda_2[1+l^2(\lambda_1^2+\lambda_2^2)](A_{12}+A_{66}),\\
S_{13}=[1+l^2(\lambda_1^2+\lambda_2^2)][B_{11}\lambda_1^3+\lambda_1\lambda_2^2(B_{12}+2B_{66})],\\
S_{14}=-[1+l^2(\lambda_1^2+\lambda_2^2)](V_{11}\lambda_1^2+V_{66}\lambda_2^2),\quad S_{15}=-\lambda_1\lambda_2[1+l^2(\lambda_1^2+\lambda_2^2)](V_{12}+V_{66}),\\
S_{16}=D_{13}\lambda_1[1+l^2(\lambda_1^2+\lambda_2^2)],\quad S_{23}=[1+l^2(\lambda_1^2+\lambda_2^2)][B_{22}\lambda_2^3+\lambda_1^2\lambda_2(B_{21}+2B_{66})],\\
S_{24}=-\lambda_1\lambda_2[1+l^2(\lambda_1^2+\lambda_2^2)](V_{21}+V_{66}),\quad S_{25}=-[1+l^2(\lambda_1^2+\lambda_2^2)](V_{66}\lambda_1^2+V_{22}\lambda_2^2),\\
S_{26}=D_{23}\lambda_2[1+l^2(\lambda_1^2+\lambda_2^2)],\quad S_{34}=[1+l^2(\lambda_1^2+\lambda_2^2)][F_{11}\lambda_1^3+\lambda_1\lambda_2^2(F_{12}+2F_{66})],\\
S_{35}=[1+l^2(\lambda_1^2+\lambda_2^2)][F_{22}\lambda_2^3+\lambda_1^2\lambda_2(F_{12}+2F_{66})],\quad S_{36}=-[1+l^2(\lambda_1^2+\lambda_2^2)](G_{13}\lambda_1^2+G_{23}\lambda_2^2),\\
S_{45}=-\lambda_1\lambda_2[1+l^2(\lambda_1^2+\lambda_2^2)](H_{12}+H_{66}),\quad S_{46}=\lambda_1[1+l^2(\lambda_1^2+\lambda_2^2)](K_{13}-M_{55}),\\
S_{56}=\lambda_2[1+l^2(\lambda_1^2+\lambda_2^2)](K_{23}-M_{44}),\quad P_{11}=P_{22}=[1+\mu^2(\lambda_1^2+\lambda_2^2)]K_1,\\
P_{13}=P_{31}=-\lambda_1K_2[1+\mu^2(\lambda_1^2+\lambda_2^2)],\quad P_{14}=P_{25}=[1+\mu^2(\lambda_1^2+\lambda_2^2)]K_4,\\
P_{23}=P_{32}=-\lambda_2K_2[1+\mu^2(\lambda_1^2+\lambda_2^2)],\quad P_{33}=[1+\mu^2(\lambda_1^2+\lambda_2^2)][K_1+K_3(\lambda_1^2+\lambda_2^2)],\\
P_{34}=-\lambda_1[1+\mu^2(\lambda_1^2+\lambda_2^2)]K_5,\quad P_{35}=-[1+\mu^2(\lambda_1^2+\lambda_2^2)]\lambda_2K_5,\quad P_{41}=P_{52}=[1+\mu^2(\lambda_1^2+\lambda_2^2)]K_4,\\
P_{43}=-[1+\mu^2(\lambda_1^2+\lambda_2^2)]\lambda_1K_5,\quad P_{44}=P_{55}=[1+\mu^2(\lambda_1^2+\lambda_2^2)]K_6,\\
P_{53}=-[1+\mu^2(\lambda_1^2+\lambda_2^2)]\lambda_2K_5,\quad P_{36}=P_{63}=[1+\mu^2(\lambda_1^2+\lambda_2^2)]K_7,\\
P_{66}=[1+\mu^2(\lambda_1^2+\lambda_2^2)]K_8,\quad (P_{12},P_{21},P_{15},P_{51},P_{16},P_{61})=0,\\
(P_{24},P_{26},P_{45},P_{46},P_{56},P_{65},P_{62},P_{64})=0.
\end{gathered} \tag{26}$$

The eigenvalue system in Eq. (25) is solved to determine the eigenfrequency values.

4. Discussions and numerical results

The accuracy and competence of the used theory (see Table 1) are observed in comparison with other analyses in the literature in this section. The certain parameters influences are investigated, such as the porosity, the geometric properties, and the power-law index. The non-dimensional parameters and the material properties are defined as follows:

- Non-dimensional parameters:

$$\widehat{\omega}=\omega h\sqrt{\frac{\rho_c}{E_c}},\quad \overline{\omega}=\omega h\sqrt{\frac{\rho_m}{E_m}}.$$

- Boundary conditions:

$$u_2 = u_3 = \phi_2 = \phi_3 = N_x = N_z = M_x = S_x = Q_{yz} = 0 \text{ at } x = 0,$$
$$u_1 = u_3 = \phi_1 = \phi_3 = N_y = N_z = M_y = S_y = Q_{xz} = 0 \text{ at } y = 0.$$

- Material properties and geometry parameters:
  - The properties of Aluminum (Al): $E_m = 70$ GPa, $\rho_m = 2702\ \mathrm{kg/m^3}$, $\nu_m = 0.3$.
  - The properties of Alumina (Al_2O_3): $E_c = 380$ GPa, $\rho_c = 3800\ \mathrm{kg/m^3}$, $\nu_c = 0.3$.
  - $p = 1$, $\mu = l = 0.1$ nm, $a/h = 10$, $a/b = 1$, $\beta = 0.1$.

To confirm the accuracy of the current formulation in predicting the dynamic response, a numerical sample is offered for the natural frequencies $\widehat{\omega}$ of an Al/Al_2O_3 FG plate with $a/h = 10$, as listed in Table 1. This example is used to examine the impacts of the power-law index. The outcomes gained from the proposed quasi-3D theory show excellent agreement with those stated by Hosseini-Hashemi et al. [31] based on the first-order shear deformation theory, El-Shahrany [33] using high-order shear/normal deformation theory, and Kenanda [30] employing a hyperbolic high-order shear deformation model. Furthermore, when the stretching effect is neglected, the present predictions closely coincide with the published data. It is also detected that the natural frequency decreases as power law indexes increase, which can be attributed to the decrease in stiffness of the FG plate caused by the higher metal content, since the metal phase has a lower Young's modulus and material density than the ceramic phase.

The fundamental frequencies of a PFGP for simply-supported conditions versus the nonlocality, the porosity coefficient, and the power law indexes are displaced in Table 2, in the absence of the strain gradient impact. As it seems, the vibrational frequency decreases by increasing the power-law parameter. On the other hand, increasing the porosity is always accompanied by a decrease in the frequency of vibration. Moreover, one can observe that the natural frequencies of PFGP also reduce with increasing the nonlocal parameter.

Table 1: Comparison of frequencies ($\widehat{\omega}$) of an FG plate for three values of power law indexes and various wave numbers.

m	n	Theory	ε_{x_3}	p = 1	4	10
1	1	FSDT [37]	= 0	0.0442	0.0382	0.0366
		HSDT [33]	≠ 0	0.0448	0.0388	0.0367
		HHSDT [40]	≠ 0	0.0450	0.0390	0.0369
		Present	≠ 0	0.0450	0.0390	0.0369
1	2	FSDT [37]	= 0	0.1059	0.0911	0.0867
		HHSDT [40]	≠ 0	0.1079	0.0925	0.0869
		Present	≠ 0	0.1081	0.0925	0.0870

Table 2: The frequencies ($\widehat{\omega}$) of a PFG plate for three power law indexes and various values of the porosity and nonlocal parameters (l = 0).

μ nm	β	p = 1	5	10
0.1	0	0.0411	0.0352	0.0337
	0.1	0.0404	0.0328	0.0313
	0.2	0.0393	0.0285	0.0270
	0.3	0.0376	0.0165	0.0128
0.3	0	0.0270	0.0231	0.0221
	0.1	0.0265	0.0215	0.0206
	0.2	0.0258	0.0187	0.0177
	0.3	0.0247	0.0108	0.0084
0.5	0	0.0185	0.0158	0.0151
	0.1	0.0181	0.0147	0.0141
	0.2	0.0176	0.0128	0.0121
	0.3	0.0169	0.0074	0.0058

Table 3 reports the fundamental frequencies of the PFG nanoplate with simply supported boundary conditions as functions of the length-scale factor, porosity coefficient, and power-law index, while accounting for nonlocal effects. The influence of the strain gradient theory is clearly reflected through variation of the length-scale factor l, where an increase in l consistently results in higher non-dimensional frequencies for all considered power-law indices. In contrast, increasing either the porosity level or the power law indexes tend to a drop in the fundamental frequencies, indicating a softening of the structural response.

Table 3: The frequencies ($\hat{\omega}$) of a PFG plate for three power law indexes and various values of the porosity and length-scale parameters ($\mu = 0.1$ nm).

l nm	β	p = 1	5	10
0.1	0	0.0450	0.0385	0.0369
	0.1	0.0442	0.0359	0.0343
	0.2	0.0430	0.0311	0.0295
	0.3	0.0411	0.0180	0.0140
0.3	0	0.0685	0.0586	0.0562
	0.1	0.0672	0.0547	0.0522
	0.2	0.0654	0.0474	0.0450
	0.3	0.0626	0.0274	0.0214
0.5	0	0.1001	0.0857	0.0822
	0.1	0.0983	0.0799	0.0763
	0.2	0.0956	0.0693	0.0658
	0.3	0.0915	0.0401	0.0312

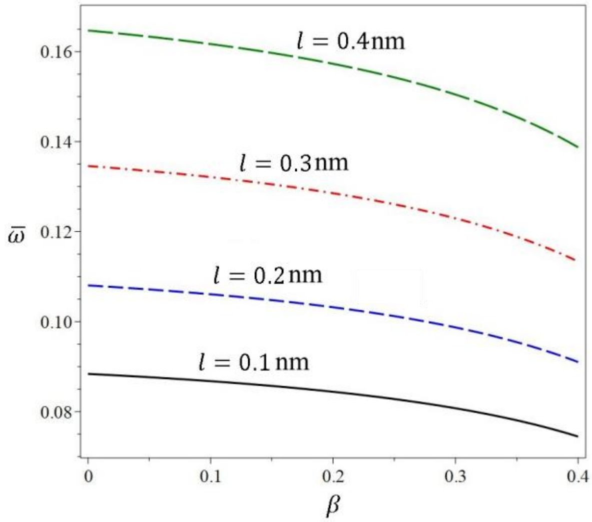

Fig. 2: Variation of frequencies versus the porosity parameters for a PFG nanoplate for different length scale parameters

Table 4: The nondimensional frequencies ($\bar{\omega}$) of a PFG nanoplate for some of the power law indexes and three values of the porosity and thickness ratios ($\mu = 0.1$ nm).

h/a	β	p = 1	5	10
0.05	0	0.0226	0.0195	0.0187
	0.1	0.0221	0.0182	0.0174
	0.2	0.0215	0.0158	0.0151
	0.3	0.0206	0.0090	0.0071
0.1	0	0.0884	0.0757	0.0725
	0.1	0.0868	0.0705	0.0674
	0.2	0.0844	0.0612	0.0581
	0.3	0.0807	0.0354	0.0276
0.15	0	0.1924	0.1625	0.1553
	0.1	0.1890	0.1514	0.1438
	0.2	0.1840	0.1314	0.1232
	0.3	0.1762	0.0770	0.0591

Figure 2 illustrates the dependency of the vibration frequency of the PFGP on the porosity coefficient for different values of the length-scale factor. The fundamental frequency increases monotonically with the length scale factor, regardless of the porosity level. Conversely, increasing the porosity results in a noticeable reduction in the frequency response.

In Table 4 impact of the thickness ratios and the porosity on the frequencies is displayed for three values of power law indexes (1, 5, and 10) and three thickness ratios (0.05, 0.1, and 0.15). Considering the tabulated findings in Table 4, the increases in the thickness ratios cause the frequency values increase irrespective of the presence or absence of porosity. In addition, it can be observed that the structure's stiffness reduces due to increasing the porosity, which tends to a decline in the frequency, and the same effect happens by raising the power law indexes.

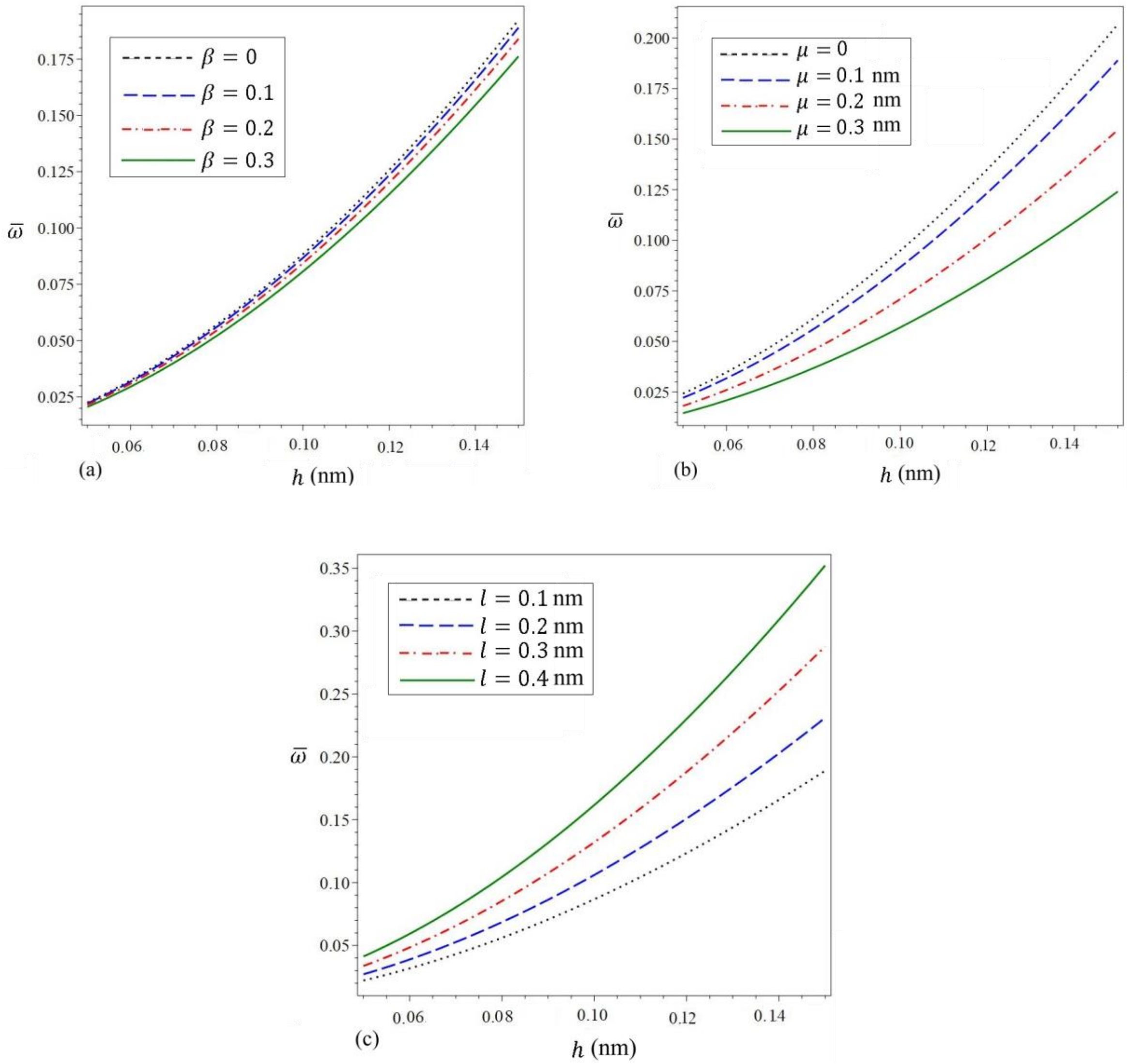

Fig. 3: Behavior of frequencies versus the thickness ratios for a PFG nanoplate (a) for some values of the porosity parameters. (b) for some values of the nonlocal parameters. (c) for different length scale parameters

Figures 3(a–c) present the variations of the frequency with respect to the thickness ratios for different combinations of porosity, nonlocal factor, and length-scale factor. The results clearly indicate that the frequency increases as the thickness ratio becomes larger. In contrast, higher values of porosity and the nonlocal factor lead to lower frequency values, while an increase in the length-scale factor produces a stiffening effect that enhances the vibrational frequency.

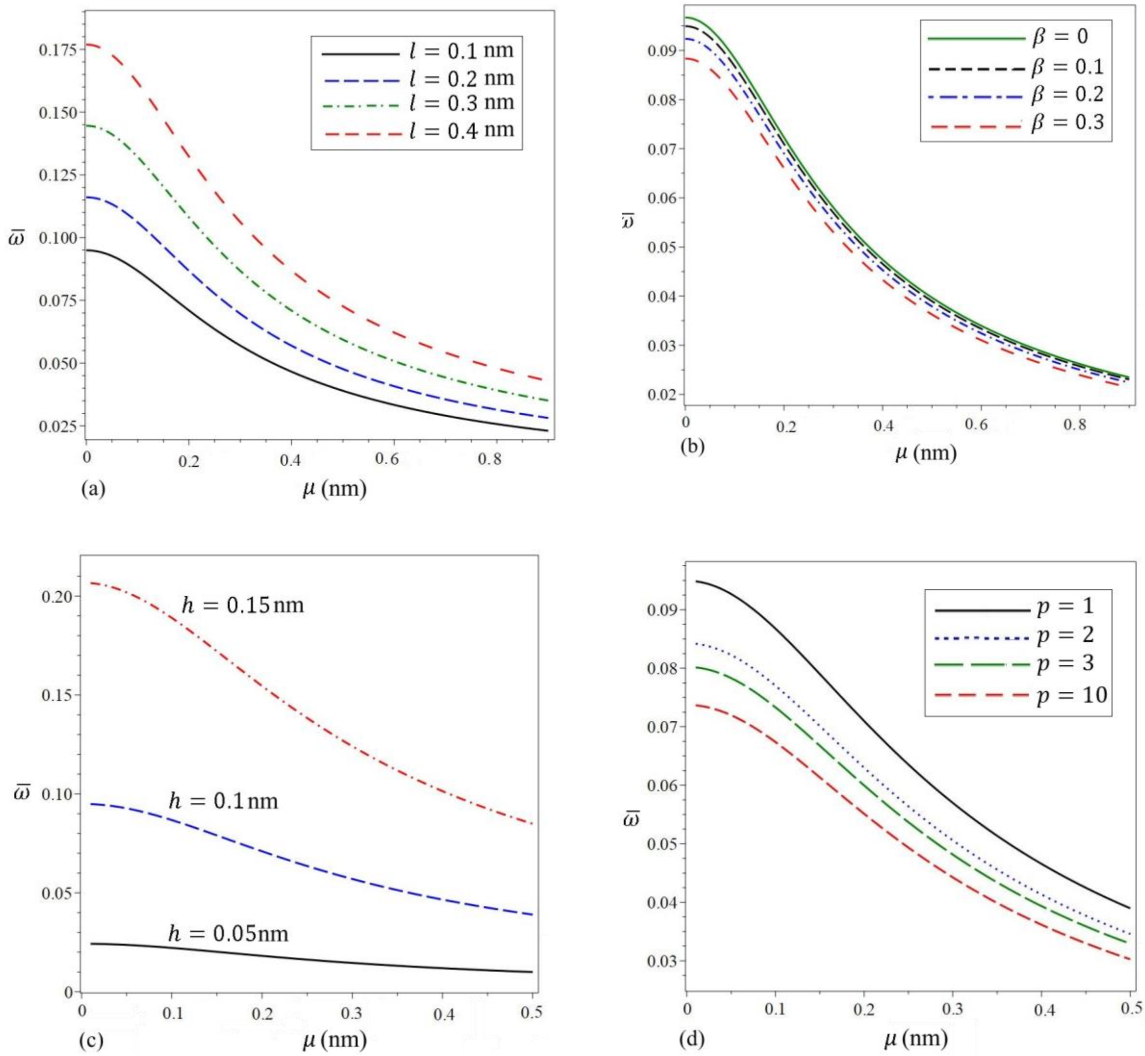

Fig. 4: The variation of frequencies versus the nonlocal parameters for a PFG nanoplate (a) for some values of the length-scale parameters. (b) for some values of the porosity parameters. (c) for some values of the thickness ratios. (d) for some values of the power indices

Figures 4(a–d) illustrate the impacts of the nonlocal factor on the fundamental frequency for various values of the length-scale factor, porosity coefficient, thickness ratios, and power law index, respectively. From these figures, it is clear that increasing the non-local factor leads to a noticeable drop in the fundamental eigenfrequency for all considered cases. In contrast, higher values of the length scale factor and the thickness ratio consistently result in increased frequency levels, reflecting their stiffening influence on the system's dynamic response. On the contrary, the frequency reduces as the porosity rises. A significant decrement in the fundamental frequency when the power indices.

Figures 5(a–d) present the variations of the nondimensional fundamental frequency of the porous FG nanoplate concerning the length scale parameter for various values of the porosity coefficient, nonlocal factor, thickness ratios, and the power indices, respectively. In all cases, the frequency curves exhibit a clear increasing trend as the length-scale factor increases, which highlights the stiffening effect introduced by the strain-gradient contribution.

In addition, the influence of material gradation is evident, as higher power-law indices consistently lead to lower frequency values due to the increased dominance of the metallic phase, which reduces the overall stiffness of the structure. A similar softening behaviour is observed with increasing porosity levels, as illustrated in Figs. 5(a-b), where higher porosity results in a noticeable decrease in the frequency response.

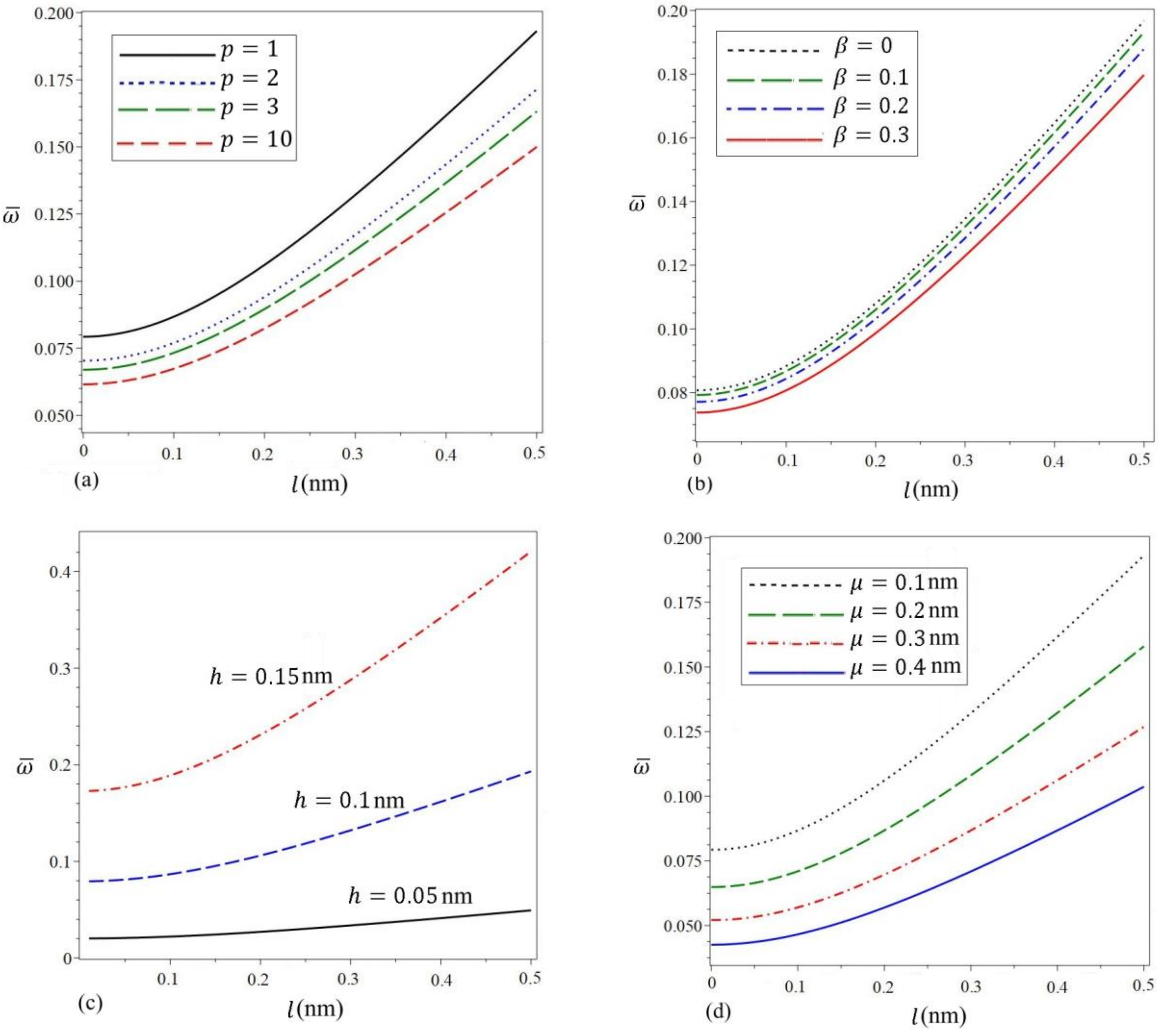

Fig. 5: Behavior of frequencies versus the length-scale factor for a PFG nanoplate (a) for some values of the power indices. (b) for some values of the porosity parameters. (c) for some values of the thickness ratios. (d) for some values of the nonlocal parameters

Conversely, Fig. 5(c) demonstrates that increasing the thickness ratio has a pronounced stiffening effect on the plate, leading to a significant rise in the non-dimensional frequency. Finally, Fig. 5(d) highlights the role of nonlocality, showing that stronger nonlocal effects reduce the fundamental frequency. This behaviour confirms that nonlocal interactions introduce an additional softening mechanism, which counteracts the stiffening influence of the length-scale factor and diminishes the overall dynamical responses of the system.

Figures 6(a-c) are plotted to display the frequency behaviour versus the porosity for different values of the power indices, the nonlocal parameters, and the thickness ratios. It is concluded that frequencies motivate decreasing by a rise in the porosities in general. Based on the diagram (Fig. 6a), frequencies gradually diminish as the power indices increase. The influence of the nonlocality is investigated by plotting the variation of frequencies versus the porosity in Fig. 6b. As mentioned before, frequencies of PFGP increase as thickness ratios rise, as shown in Fig. 6c.

5. Conclusions

This study provides an in-depth theoretical examination of the elastic vibration characteristics of PFG plates. The governing formulation is established within the framework of linear elasticity by accounting for the stretching effect through a hyperbolic shear deformation model, thereby evading the use of shear correction factors. The resulting vibration eigenvalue problem of the PFGP is solved analytically using Navier's solution approach, offering an efficient and reliable means for evaluating the dynamic response of the structure.

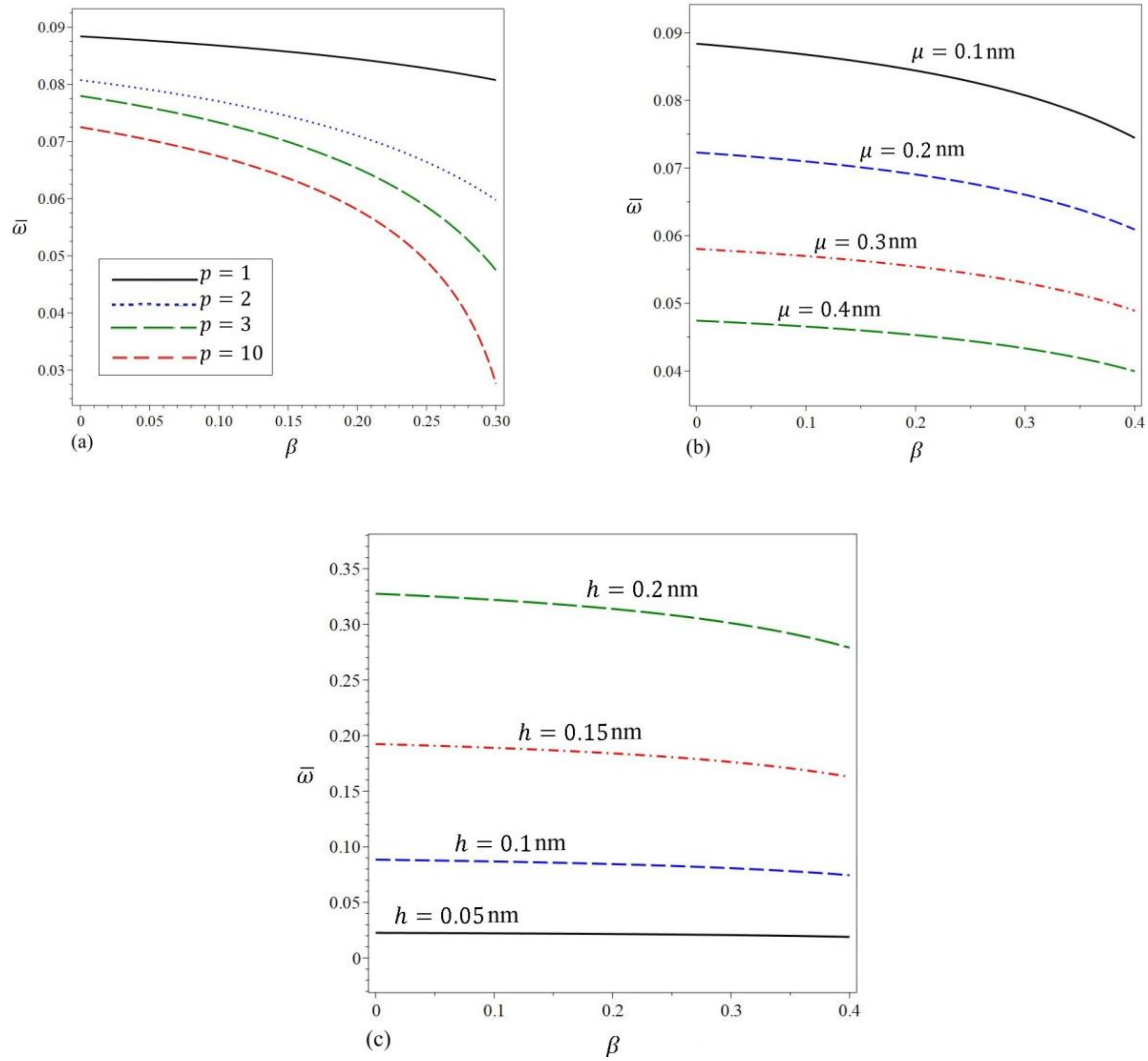

Fig. 6: The variation of frequencies versus the porosity parameters for a PFG nanoplate (a) for some values of power indices. (b) for some values of the nonlocal parameters. (c) for some values of the thickness ratios

Comprehensive parametric revisions are approved to assess the impacts of key material and structural parameters, including porosity coefficient, nonlocal parameter, material length-scale factor, thickness ratio, and power-law index, on the non-dimensional fundamental frequency. The numerical results demonstrate that the vibrational characteristics of PFGPs are strongly influenced by the combined effects of porosity distribution, nonlocal elasticity, strain-gradient effects, and material gradation.

Comparisons with previously published results available in the literature show excellent agreement, confirming the validity and reliability of the current formulation. The findings indicate that the rising value of the power indices results in a reduction in the fundamental eigenfrequency, both in porous and non-porous configurations, due to the increased contribution of the metal phase and the associated reduction in stiffness. In contrast, increasing the thickness ratio enhances the structural rigidity, resulting in higher frequency values.

Moreover, the presence of porosity significantly degrades the stiffness and mechanical performance of the PFGP, leading to lower vibration frequencies and increasing the susceptibility of the structure to damage, such as cracking or fracture. These observations emphasize the importance of controlling porosity during the manufacturing process of FG materials. Consequently, advanced fabrication techniques that limit porosity content are strongly recommended to improve the structural integrity and dynamic performance of FGM-based components.

Overall, the present study delivers useful insights into the dynamic behaviour of PFG nanoplates and can serve as a reliable reference for the design and optimization of advanced micro- and nano-scale structural elements.

Appendix A

- The stress resultants N, M, S, and Q are defined by:

$$\left(N_x, N_y, N_{xy}\right) = \int_{-h/2}^{h/2} \left(\sigma_x, \sigma_y, \tau_{xy}\right) \mathrm{d}z, \quad N_z = \int_{-h/2}^{h/2} F''(z) \sigma_z \mathrm{d}z,$$

$$\left(M_x, M_y, M_{xy}\right) = \int_{-h/2}^{h/2} z\left(\sigma_x, \sigma_y, \tau_{xy}\right) \mathrm{d}z,$$

$$\left(S_x, S_y, S_{xy}\right) = \int_{-h/2}^{h/2} F(z)\left(x, \sigma_y, \tau_{xy}\right) \mathrm{d}z,$$

$$\left(Q_{xz}, Q_{yz}\right) = \int_{-h/2}^{h/2} F'(x_3)\left(\tau_{xz}, \tau_{yz}\right) \mathrm{d}x.$$

- The moment of inertia is defined as:

$$T_i = \int_{-h/2}^{h/2} \left[1, z, (z)^2, F(z), zF(z), \left(F(z)\right)^2, F'(z), (F'(z))^2\right] \rho(z) \mathrm{d}z, \ i = 1, \ldots, 8.$$

- The stiffness terms (A_{ij}, B_{ij}, E_{ij}, V_{ij}, F_{ij}, H_{ij}, D_{ij}, G_{ij}, K_{ij}, M_{ij}, L_{ij}) are defined as:

$$(A_{11}, A_{22}, A_{12}, A_{66}) = \int_{-h/2}^{h/2} (\tilde{c}_{11}, \tilde{c}_{22}, \tilde{c}_{12}, \tilde{c}_{66})\, \mathrm{d}z,$$

$$(B_{11}, B_{22}, B_{12}, B_{66}) = \int_{-h/2}^{h/2} (\tilde{c}_{11}, \tilde{c}_{22}, \tilde{c}_{12}, \tilde{c}_{66})\, z\mathrm{d}z,$$

$$(E_{11}, E_{22}, E_{12}, E_{66}) = \int_{-h/2}^{h/2} (\tilde{c}_{11}, \tilde{c}_{22}, \tilde{c}_{12}, \tilde{c}_{66})\, (z)^2 \mathrm{d}z,$$

$$(V_{11}, V_{22}, V_{12}, V_{66}) = \int_{-\frac{h}{2}}^{\frac{h}{2}} (\tilde{c}_{11}, \tilde{c}_{22}, \tilde{c}_{12}, \tilde{c}_{66})\, F(z) \mathrm{d}z,$$

$$(F_{11}, F_{22}, F_{12}, F_{66}) = \int_{-h/2}^{h/2} (\tilde{c}_{11}, \tilde{c}_{22}, \tilde{c}_{12}, \tilde{c}_{66})\, zF(z) \mathrm{d}z,$$

$$(H_{11}, H_{22}, H_{12}, H_{66}) = \int_{-h/2}^{h/2} (\tilde{c}_{11}, \tilde{c}_{22}, \tilde{c}_{12}, \tilde{c}_{66})\, F^2(z) \mathrm{d}z,$$

$$(D_{31}, D_{32}) = \int_{-h/2}^{h/2} (\tilde{c}_{31}, \tilde{c}_{32}) F''(z)\, \mathrm{d}z,$$

$$(G_{31}, G_{32}) = \int_{-h/2}^{h/2} (\tilde{c}_{31}, \tilde{c}_{32}) x_3 F''(z)\, \mathrm{d}z,$$

$$(K_{13}, K_{23}) = \int_{-h/2}^{h/2} (\tilde{c}_{13}, \tilde{c}_{23})\, F(z) F''(z)\, \mathrm{d}z,$$

$$(M_{44}, M_{55}) = \int_{-h/2}^{h/2} (\tilde{c}_{44}, \tilde{c}_{55}) [F'(z)]^2\, \mathrm{d}z.$$

Acknowledgments

The authors are thankful to the Deanship of Graduate Studies and Scientific Research at University of Bisha for supporting this work through the Fast-Track Research Support Program.

References

[1] J. Reddy, Analysis of functionally graded plates, *International Journal for Numerical Methods in Engineering - INT J NUMER METHOD ENG,* Vol. 47, pp. 663-684, 01/10, 2000.

[2] J. Reddy, J. I. Barbosa, On vibration suppression of magnetostrictive beams, *Smart Materials and Structures,* Vol. 9, pp. 49, 02/22, 2000.

[3] J. Reddy, C. Wang, G. Lim, K. Ng, Bending solutions of Levinson beams and plates in terms of the classical Theories, *International Journal of Solids and Structures - INT J SOLIDS STRUCT,* Vol. 38, pp. 4701-4720, 06/01, 2001.

[4] M. Touratier, An efficient standard plate theory, *International Journal of Engineering Science,* Vol. 29, No. 8, pp. 901-916, 1991/01/01/, 1991.

[5] J. Mantari, A. Oktem, C. G. Soares, A new trigonometric shear deformation theory for isotropic, laminated composite and sandwich plates, *International Journal of Solids and Structures,* Vol. 49, No. 1, pp. 43-53, 2012.

[6] A. M. A. Neves, A. J. M. Ferreira, E. Carrera, C. M. C. Roque, M. Cinefra, R. M. N. Jorge, C. M. M. Soares, A quasi-3D sinusoidal shear deformation theory for the static and free vibration analysis of functionally graded plates, *Composites Part B: Engineering,* Vol. 43, No. 2, pp. 711-725, 2012/03/01/, 2012.

[7] C. Abdelbaki, Investigations in static response and free vibration of a functionally graded beam resting on elastic foundations, *Frattura ed Integrità Strutturale,* Vol. 14, pp. 115-126, 12/04, 2019.

[8] A. M. Zenkour, A simple four-unknown refined theory for bending analysis of functionally graded plates, *Applied Mathematical Modelling,* Vol. 37, No. 20, pp. 9041-9051, 2013/11/01/, 2013.

[9] D. Shahsavari, M. Shahsavari, L. Li, B. Karami, A novel quasi-3D hyperbolic theory for free vibration of FG plates with porosities resting on Winkler/Pasternak/Kerr foundation, *Aerospace Science and Technology,* Vol. 72, pp. 134-149, 2018/01/01/, 2018.

[10] A. Garg, T. Mukhopadhyay, M. O. Belarbi, H. D. Chalak, A. Singh, A. M. Zenkour, On accurately capturing the through-thickness variation of transverse shear and normal stresses for composite beams using FSDT coupled with GPR, *Composite Structures,* Vol. 305, pp. 116551, 2023/02/01/, 2023.

[11] S. S. Akavci, A. H. Tanrikulu, Static and free vibration analysis of functionally graded plates based on a new quasi-3D and 2D shear deformation theories, *Composites Part B: Engineering,* Vol. 83, pp. 203-215, 2015/12/15/, 2015.

[12] Y. S. Joshan, S. Santapuri, N. Grover, Analysis of laminated piezoelectric composite plates using an inverse hyperbolic coupled plate theory, *Applied Mathematical Modelling,* Vol. 82, pp. 359-378, 2020/06/01/, 2020.

[13] A. M. A. Neves, A. J. M. Ferreira, E. Carrera, M. Cinefra, C. M. C. Roque, R. M. N. Jorge, C. M. M. Soares, A quasi-3D hyperbolic shear deformation theory for the static and free vibration analysis of functionally graded plates, *Composite Structures,* Vol. 94, No. 5, pp. 1814-1825, 2012/04/01/, 2012.

[14] Q.-H. Pham, V. Ke Tran, T. Thanh Tran, V. Chinh Nguyen, A. M. Zenkour, Nonlocal higher-order finite element modeling for vibration analysis of viscoelastic orthotropic nanoplates resting on variable viscoelastic foundation, *Composite Structures,* Vol. 318, pp. 117067, 2023/08/15/, 2023.

[15] S. Sarangan, B. N. Singh, Higher-order closed-form solution for the analysis of laminated composite and sandwich plates based on new shear deformation theories, *Composite Structures,* Vol. 138, pp. 391-403, 2016/03/15/, 2016.

[16] K. P. Soldatos, A transverse shear deformation theory for homogeneous monoclinic plates, *Acta Mechanica,* Vol. 94, No. 3, pp. 195-220, 1992/09/01, 1992.

[17] A. M. Zenkour, H. D. El-Shahrany, Quasi-3D theory for the vibration and deflection of a magnetostrictive composite plate resting on a viscoelastic medium, *Composite Structures,* Vol. 269, pp. 114028, 2021/08/01/, 2021.

[18] M. Malikan, V. A. Eremeyev, A new hyperbolic-polynomial higher-order elasticity theory for mechanics of thick FGM beams with imperfection in the material composition, *Composite Structures,* Vol. 249, pp. 112486, 2020/10/01/, 2020.

[19] Y. Khalfi, A. Bouchikhi, Y. Bellebna, Mechanical Stability Investigation of Advanced Composite Plates Resting on Elastic Foundations Using a New Four-Unknown Refined Theory, *Frattura ed Integrità Strutturale,* Vol. 13, pp. 208-221, 03/05, 2019.

[20] M. Aydogdu, A new shear deformation theory for laminated composite plates, *Composite Structures - COMPOS STRUCT,* Vol. 89, pp. 94-101, 06/01, 2009.

[21] H.-T. Thai, D.-H. Choi, Improved refined plate theory accounting for effect of thickness stretching in functionally graded plates, *Composites Part B: Engineering,* Vol. 56, pp. 705-716, 2014/01/01/, 2014.

[22] M. Bouazza, A. Zenkour, Hygrothermal environmental effect on free vibration of laminated plates using nth-order shear deformation theory, *Waves in Random and Complex Media,* Vol. 34, pp. 1-17, 04/05, 2021.

[23] S. Merdaci, A. H. Mostefa, Influence of porosity on the analysis of sandwich plates FGM using of high order shear-deformation theory, *Fracture and Structural Integrity,* Vol. 14, No. 51, pp. 199-214, 11/25, 2019.

[24] P. V. Vinh, A. M. Zenkour, Vibration analysis of functionally graded sandwich porous plates with arbitrary boundary conditions: a new general viscoelastic Winkler–Pasternak foundation approach, *Eng. with Comput.,* Vol. 41, No. 6, pp. 4125–4153, 2025.

[25] N. Hebbar, I. Hebbar, D. Ouinas, M. Bourada, Numerical modeling of bending, buckling, and vibration of functionally graded beams by using a higher-order shear deformation theory, *Frattura ed Integrità Strutturale,* Vol. 14, pp. 230-246, 03/03, 2020.

[26] M. Rabehi, R. Billel, M. Meradjah, A. Zenkour, Porosity Investigations on Dynamic Responses of FG Plates via a Modified Quasi-3D Shear Deformation Theory, *Journal of Vibration Engineering & Technologies,* Vol. 141, 01/22, 2025.

[27] H. D. El-Shahrany, Porosity-Dependent Frequency Analysis of Bidirectional Porous Functionally Graded Plates via Nonlocal Elasticity Theory, *Mathematics,* Vol. 13, No. 16, pp. 2688, 2025.

[28] l. thanh cuong, K. Nguyen, N. Nguyen, S. Khatir, H. Nguyen-Xuan, M. Abdel Wahab, A three-dimensional solution for free vibration and buckling of annular plate, conical, cylinder and cylindrical shell of FG porous-cellular materials using IGA, *Composite Structures,* Vol. 31 October 2020, 10/31, 2020.

[29] M. Slimane, A. Hadj Mostefa, O. Khayal, Natural frequencies of FG plates with two new distribution of porosity, *International Journal of Applied Mechanics and Engineering,* Vol. 26, pp. 128-142, 06/27, 2021.

[30] M. Kenanda, F. Hammadi, Z. Belabed, M. Meliani, Free vibration analysis of porous functionally graded plates using a novel Quasi-3D hyperbolic high order shear deformation theory, *Frattura ed Integrità Strutturale,* Vol. 64, pp. 266-282, 2023.

[31] S. Hosseini-Hashemi, M. Fadaee, S. R. Atashipour, A new exact analytical approach for free vibration of Reissner–Mindlin functionally graded rectangular plates, *International Journal of Mechanical Sciences,* Vol. 53, No. 1, pp. 11-22, 2011/01/01/, 2011.

[32] F. Ebrahimi, M. Barati, A. Dabbagh, A nonlocal strain gradient theory for wave propagation analysis in temperature-dependent inhomogeneous nanoplates, *International Journal of Engineering Science,* Vol. 107, pp. 169-182, 10/01, 2016.

[33] F. Ebrahimi, A. Dabbagh, Viscoelastic wave propagation analysis of axially motivated double-layered graphene sheets via nonlocal strain gradient theory, *Waves in Random and Complex Media,* Vol. 30, pp. 1-20, 07/02, 2018.

[34] P. Hoa, N. Hoàng Thịnh, T. Ke, A. Zenkour, Hygro-thermo-mechanical vibration analysis of functionally graded porous curved nanobeams resting on elastic foundations, *Waves in Random and Complex Media*, pp. 1-32, 02/16, 2023.

[35] H. El-Shahrany, A. Zenkour, A nonlocal vibration suppression for a multilayered magneto-viscoelastic nanobeam on a three-parameter-type medium, *Mechanics of Advanced Materials and Structures,* Vol. 31, pp. 1-12, 11/22, 2023.